RESEARCH ARTICLE

Open Access

$OONO^-$ reduces the expression of steroidogenic genes and proteins to inhibit estrogen secretion in porcine ovarian granulosa cells

2025 Volume 2, Article number: e031

https://doi.org/10.48130/animadv-0025-0028

Received: 6 February 2025

Revised: 23 May 2025

Accepted: 28 May 2025

Published online: 3 November 2025

Yue Zhang[1#], Kun Lei[1#], Zhe Wang[1], Fang Zhao[2], Jun Xing[3], Shanli Zhu[1], Yongsheng Li[1], Shuang Li[1], Wei Ding[3] and Quanwei Wei[1,4*]

[1] College of Animal Science and Technology, Nanjing Agricultural University, Nanjing 210095, China
[2] Institute of Animal Science, Jiangsu Academy of Agricultural Sciences, Nanjing 210014, China
[3] Animal Husbandry and Veterinary College, Jiangsu Vocational College Agriculture and Forestry, Jurong 212400, China
[4] School of Medicine, University of Virginia, Charlottesville 22901, USA
[#] Authors contributed equally: Yue Zhang, Kun Lei
* Corresponding author, E-mail: weiquanwei@njau.edu.cn

Citation: Zhang Y, Lei K, Wang Z, Zhao F, Xing J, et al. 2025. $OONO^-$ reduces the expression of steroidogenic genes and proteins to inhibit estrogen secretion in porcine ovarian granulosa cells. *Animal Advances* 2: e031 https://doi.org/10.48130/animadv-0025-0028

Abstract

Granulosa cells (GCs), as critical somatic components of ovarian follicles, maintain female reproductive physiology through steroid hormone regulation and follicular development. To investigate the effects of the peroxynitrite anion ($OONO^-$) on GCs' function and estrogen (E_2) secretion in sows, GCs were treated with 3-morpholinosydnonimine (SIN-1, an $OONO^-$ donor), with subsequent validation using carboxy-PTIO (cPTIO, a NO scavenger) to confirm $OONO^-$-specific effects. RNA sequencing (RNA-seq) revealed that $OONO^-$-induced transcriptional alterations in GCs, with Gene Ontology (GO) and Kyoto Encyclopedia of Genes and Genomes (KEGG) analyses revealing significant pathway disruptions, including estrogen metabolism and cellular proliferation. The mechanism of the effect of $OONO^-$ on GCs' E_2 secretion was further explored. The experimental data showed that $OONO^-$ inhibited E_2 secretion by significantly downregulating key steroidogenic regulators (CYP19A1, 3β-HSD, and follicle-stimulating hormone receptor [FSHR]). In conclusion, this study indicated that $OONO^-$ impairs GCs physiological functions via molecular network dysregulation, leading to inhibited E_2 secretion and affecting follicular development.

Introduction

'The reproductive performance of sows, a critical economic determinant in livestock production, mainly depends on ovarian physiological function and follicular development[1]. Granulosa cells (GCs) are important somatic cells in the ovaries[2]. The primary roles of GCs are impacting follicular development and taking part in the secretion of steroid hormones[3,4]. GC apoptosis has been recognized as the primary cause of follicular atresia[5,6]. In addition, GCs can also secrete steroid hormones such as estrogen (E_2) and progesterone (P_4) to regulate follicular maturation[7]. E_2 can work together with follicle-stimulating hormone (FSH) to enhance GCs' proliferation through autocrine signaling[8]. E_2 also increases the synthesis of luteinizing hormone receptor (LHR) and aromatase, thereby inhibiting GC apoptosis and promoting follicular development[9,10]. In contrast, P_4 plays an important role in maintaining pregnancy, promoting full development of the genital tract, inhibiting estrus and ovulation, and decreasing cell apoptosis[11–15]. Steroid hormones secreted by GCs play important roles in determining follicular fate, positioning their functional analysis as a strategic approach to enhance female reproductive efficiency.

Nitric oxide (NO), a gaseous signaling molecule synthesized by nitric oxide synthase (NOS), serves as a critical regulator of physiological and pathological processes through redox-dependent mechanisms[16–18]. NOS is expressed in mammalian ovaries[19,20]. Within this physiological context, NO regulates key reproductive processes, including hormone regulation[21–23], pregnancy maintenance, and labor[24]. Previous studies have revealed a concentration-dependent duality in NO's bioactivity[25]. At physiological levels, NO inhibits apoptosis and promotes follicular development[26,27], while supraphysiological concentrations trigger oocyte apoptosis and follicular atresia. However, the relevant mechanisms need to be further studied.

In the organism, high concentrations of NO may react with the superoxide anion (O_2^-) to produce the peroxynitrite anion ($OONO^-$)[28,29]. Compared with NO, $ONOO^-$ demonstrates strong oxidative capacity, generating additional reactive species and exerting extensive tissue-damaging effects[30], These include promoting lipid peroxidation and nitration[31], inactivating enzymes[32], and impairing mitochondrial respiration via protein oxidation and nitration. In particular, oxidative stress reduces the synthesis of FSH-maintained GC steroid hormones, primarily E_2, a critical ovarian response biomarker[33]. In addition, $OONO^-$ is considered to very readily mediate protein tyrosine nitration (PTN) in cells. PTN is a stable post-translational modification of proteins, which plays an important role in the occurrence of many diseases. This cellular toxicity primarily arises from $ONOO^-$'s ability to nitrate tyrosine residues. Franco et al. found, in PC12 cells, that $ONOO^-$-induced Hsp90 tyrosine nitration disrupts cellular functions: nitration at tyrosine 56 triggers apoptosis, while a modification at Residue 33 compromises mitochondrial activity[34,35]. The resulting formation of 3-nitrotyrosine (3-NT) serves as a reliable biomarker for endogenous protein nitration.

Previous studies have demonstrated that $OONO^-$ induces DNA damage in GCs and inhibits DNA repair through MMP-2/MMP-9-mediated impairment of PARP1 activity, ultimately resulting in GC apoptosis[36]. However, the potential impact of accumulating $ONOO^-$

on GC's functions and steroid hormone secretion remains uncharacterized.

Therefore, this study employed the $OONO^-$ donor SIN-1 to treat GCs, utilizing RNA sequencing (RNA-seq) to investigate $OONO^-$-mediated alterations in GCs' physiological functions. The effects of $OONO^-$ on GCs' E_2 secretion were assessed through enzyme-linked immunosorbent assay (ELISA), combined with molecular analyses of the expression of E_2 synthesis-associated proteins and genes. Furthermore, the NO scavenger cPTIO was applied to validate the functional role of $OONO^-$.

Materials and methods

Follicle classification and collection

Ovaries from non-pregnant sows were obtained from a slaughterhouse (Changzhou Erhualian Pig Production Cooperation, Jiangsu, China). The ovaries were preserved in sterile saline (0.9%) containing 100 IU/mL penicillin and 100 μg/mL streptomycin (Solarbio, Beijing, China) within vacuum-sealed flasks and transported to the laboratory within 2 h. Follicles were morphologically classified under a surgical dissecting microscope (SZ40; Olympus Corporation, Tokyo, Japan) into three categories according to established criteria: healthy follicles (H), early atretic follicles (EA), and progressively atretic follicles (PA)[37]. Briefly, healthy follicles have a pinkish-red coloration, dense vascularization, and clear follicular fluid, while EA follicles display reduced or absent surface vascularization with mildly turbid follicular fluid. The follicles of the PA group present a grayish-white appearance, no vascularization, and opaque follicular fluid.

Isolation, culture, and identification of porcine ovarian granulosa cells

Ovaries were transported to the laboratory to isolate GCs. Ovaries were rinsed with saline, a 75% ethanol solution, and saline containing 1% penicillin–streptomycin (P/S), all of which were rinsed two or three times to eliminate residual blood. Follicular fluid was aspirated using sterile syringes and transferred to enzyme-free centrifuge tubes. After centrifugation (1,500 *g*, 5 min), the supernatants were discarded, and the GCs were washed two or three times with phosphate-buffered saline (PBS) containing 1% P/S. Cells were resuspended in Dulbecco's Modified Eagle's Medium/Nutrient Mixture F-12 (DEME/F) (WISENT, 319-085-CL) containing 10% fetal bovine serum (FBS) (Omega, FB-21-311892) and a 1% P/S solution. They were maintained in an incubator (37 °C, 5% CO_2). Non-adherent cells were removed through replacement of the medium at 24 h. Immunofluorescence staining was performed according to Yousefi et al.[38]. Stained specimens were analyzed using an inverted fluorescence microscope (Axiovert 40C/CFL, Zeiss) after mounting.

When the GCs' confluency in a six-well plate reached 80% to 90% (about 5×10^5 cells/well), 3-morpholinosydnonimine (SIN-1) (Santa Cruz Biotechnology, sc-200339) or carboxy-PTIO (cPTIO) (Beyotime Biotechnology, S1546) was added to the medium containing 5% serum for cell treatment. The treatment concentration of SIN-1 was determined by a CCK-8 experiment. cPTIO, a NO scavenger, was added to the medium at a concentration of 100 μM to treat GCs half an hour before the SIN-1 treatment. After treatment, the GCs were washed with PBS containing 1% P/S and collected for further experimental analysis.

CCK-8 assay

A CCK-8 assay was used to detect the cell viability of GCs subjected to different treatments. The assay was carried out in strict accordance with the instructions of the CCK-8 kit (Apexbio, K1018), and the specific steps were as follows: GCs were seeded in 96-well plates and cultured to 70%–80% confluency prior to treatment with SIN-1 at increasing concentrations (including 0, 100, 200, 400, 600, 800, and 1,000 μM). Treated cells were incubated for 24 h under standard culture conditions (37 °C, 5% CO_2). Following treatment, the culture medium was replaced with a freshly prepared CCK-8 working solution (10:1 ratio of culture medium to CCK-8 reagent; 100 μL per well). After a 2-h incubation period, absorbance measurements were conducted at 450 nm.

ELISA

Estrogen concentrations in the cell culture supernatants and follicular fluid were quantified using an ELISA kit (Nanjing Xin Fan Biology, XFP40451) following the manufacturer's protocol. The assay demonstrated a detection sensitivity of 1.83 pg/mL for E_2, with the intra- and inter-assay coefficients of variation maintained below 10% and 15%, respectively, ensuring analytical precision. The specific assay steps followed the ELISA kit's instructions.

Western blot analysis

Total protein was extracted using a radioimmunoprecipitation analysis (RIPA) lysis buffer (Apexbio, K1020). Protein concentrations were quantified with a bicinchoninic acid (BCA) kit (Boster Bio, AR1189).

Protein lysates were normalized to equal concentrations by adjusting the volumes of the RIPA buffer and the sodium dodecyl sulfate (SDS) loading buffer (Ncmbio, Suzhou, China), followed by denaturation at 100 °C for 10 min. Denatured samples were separated on 4%–20% Sure polyacrylamide gel electrophoresis (PAGE) gels (Genscript, Nanjing, China) and electrophoretically transferred to 45-μm polyvinylidene fluoride (PVDF) membranes (Millipore). PVDF membranes were blocked with 5% BSA for 1.5 h at ambient temperature prior to overnight incubation with primary antibodies (Table 1) at 4 °C. After three 5-min Tris-buffered saline–Tween (TBST) washes, the membranes were then incubated with secondary antibodies for 1 h at room temperature, followed by three additional TBST washes. Protein bands were visualized using an enhanced chemiluminescence (ECL) substrate (Biosharp, Hefei, China), and imaged with a ultrasensitive chemiluminescence gel imaging system (Bio-Rad). Band intensity quantification was performed using ImageJ.

RNA extraction and cDNA synthesis

Total RNA was isolated from treated GCs using Trizol reagent (Invitrogen, Carlsbad, CA, USA) following the manufacturer's protocol. RNA purity and concentration were quantified using a nucleic acid protein assay on an ND-2000 spectrophotometer (Nano Drop Technologies, Wilmington, DE, USA). Qualified RNA samples underwent reverse transcription using a reverse transcription kit (Vazyme, R233-01). Synthesized cDNA was stored at −20 °C.

RNA-seq and bioinformatic analysis

After extraction of total RNA, poly(A) mRNA isolation was performed using Oligo (dT) beads. mRNA fragmentation was achieved through divalent cation-mediated cleavage at a high temperature. First-strand cDNA and second-strand cDNA were synthesized by reverse transcription using random primers. The purified double-stranded cDNA was then processed by repairing both ends and adding a dA-tailing in one reaction, followed by a T-A ligation to add adaptors to both ends.

Table 1. Primary antibodies.

Primary antibody	Purpose	Dilution	Source	Cat No.
Cleaved Caspase-3 pAb	WB	1:1,000	Cell Signaling	#9661L
β-actin pAb	WB	1:5,000	Affinity	#AF7018
CYP19A1 pAb	WB	1:1,000	CST	#14528
GAPDH pAb	WB	1:10,000	Affinity	#AF7021
FSHR pAb	WB	1:1,000	Abclone	A3172
CYP11A1 pAb	WB	1:1,000	Santa	A1713
HSD3*β* pAb	WB	1:1,000	Santa	sc-515120
STAR pAb	WB	1:1,000	Santa	sc-166821
3-Nitrotyrosine mAb	WB	1:1,000	Abcam	ab110282

Adapter ligation DNA size selection was then performed using DNA Clean Beads. Each sample was amplified by polymerase chain reaction (PCR) with P5 and P7 primers, and the PCR products were validated.

The differently indexed libraries were then multiplexed and loaded on an Illumina HiSeq/Illumina Novaseq/MGI2000 instrument for sequencing using a 2 × 150 paired-end (PE) configuration. Differential gene expression analysis was conducted using DESeq2, identifying transcripts with an adjusted p-value of < 0.05, a false discovery rate (FDR) of ≤ 0.05, and an absolute $\log_2$ fold change (FC) of > 1 as differentially expressed genes (DEGs). To determine the biological pathways and functions of the DEGs, Gene Ontology (GO) and Kyoto Encyclopedia of Genes and Genomes (KEGG) analyses were performed on the DEGs. The GO annotation tems were acquired through Goseq (v1.34.1), followed by implementation of GO functional enrichment analysis.

Quantitative reverse transcription-PCR

Quantitative reverse transcription-PCR (qPCR) analysis was performed using synthesized cDNA templates with a kit (Vazyme, Q111-02/03). The system of the reaction mixture (total volume = 20 μL) is shown in Table 2.

Quantitative PCRs were performed as follows: initial denaturation at 95 °C for 30 s, followed by 40 cycles of 10 s at 95 °C and 30 s at 60 °C. Melt curve analysis was conducted through sequential incubations at 95 °C (15 s), 60 °C (60 s), and 95 °C (15 s). Information on the primers used in this study is shown in Table 3. The target genes' expression levels were normalized to *GAPDH* as an endogenous control and quantified via the $2^{-\Delta\Delta Ct}$ method.

Statistical analysis

All experiments were repeated at least three times ($n \geq 3$). Statistical analyses were conducted using SPSS 24.0 (SPSS Inc. Chicago, IL, USA) with the data presented as the mean ± standard error of the mean (SEM). One-way analysis of variance (ANOVA) and Student's t-test were used to test the significance of the differences. All of the statistical analyses were verified by Tukey's *post hoc* test. Significance thresholds were established at $p < 0.05$ (significant) and $p < 0.01$ (extremely significant). Data visualization was performed using GraphPad Prism 9 (GraphPad Prism 9.Ink, Boston, MA, USA).

Results

Follicle classification

Follicles were classified into three distinct atresia stages, namely healthy (H), early atretic (EA), and progressively atretic (PA), according to established morphological criteria (Fig. 1a)[37]. Apoptotic activity in the GCs across follicular categories was assessed through Cleaved Caspase-3 detection via immunohistochemistry (IHC) and Western blotting. As shown in Fig. 1b, the expression of Cleaved Caspase-3 was significantly increased in EA and PA follicles compared with the H group. In addition, the IHC results showed that the expression of Cleaved Caspase-3 in paraffin sections increased with follicular atresia (Fig. 1c). All these results suggested that GC apoptosis was associated with follicular atresia, and demonstrated the reliability of our classification for further experiments.

Table 2. Real-time qualitative PCR system.

Components	Volume (μL)
2 × ChamQ SYBR qPCR Master Mix	10
Forward primer	0.4
Reverse primer	0.4
50× ROX reference dye	0.4
cDNA template	2
Nuclease-free water	6.8

The estrogen secretion level of granulosa cells decreased during follicular atresia

E_2 secretion dynamics during follicular atresia were quantified through follicular fluid analysis using ELISA. PA follicles exhibited a reduction in E_2 concentration compared with H follicles, while EA follicles showed an intermediate decrease that did not reach statistical significance (Fig. 2a). The RNA-seq data were then used to screen for GO functions containing the terms 'estrogen', 'steroid', and 'hormone', and the genes with significant differences ($p < 0.05$) were screened (Fig. 2b). The results showed that in PA, the expression levels of estrogen synthesis-related genes such as *CYP19A1* and *STAR* were significantly decreased. The expression levels of steroid hormone secretion-related proteins in different classes of follicles were examined further. With follicular atresia, the expression of CYP19A1 and follicle-stimulating hormone receptor (FSHR) proteins decreased significantly (Fig. 2c). These results indicated that GCs diminished the capacity for E_2 synthesis during follicular degeneration.

Isolation and characterization of porcine ovarian GCs

GCs were isolated from porcine ovaries and cultured for subsequent experiments. Inverted microscopy revealed a characteristic GC morphology, displaying uniform spindle-shaped cellular structures (Fig. 3a). To confirm cellular identity, immunofluorescence staining was performed for FSHR, a GC-specific marker. As shown in Fig. 3b, FSHR-specific green fluorescence co-localized with nuclear 4′,6-diamidino-2-phenylindole (DAPI) staining (blue). More than 90% of the cells in the random field of view were positive for FSHR expression, verifying successful isolation of high-purity GCs suitable for subsequent experiments.

Concentration-dependent effects of OONO⁻ on GCs' function

To evaluate OONO⁻-mediated effects on GCs' functionality, GCs were treated with SIN-1 (an OONO⁻ donor). Previous experimental data revealed concentration-dependent decreases in GCs' viability following 24 h of exposure to SIN-1[36]. CCK-8 assays confirmed this trend (Fig. 4): 600 μM SIN-1 significantly reduced GCs' viability, while treatment with 800 μM decreased viability by over 50%. Three concentration-based experimental groups were selected for RNA-seq: (1) 0 μM (control), (2) 400 μM (pre-significance exposure level), and (3) 800 μM (> 50% viability loss). DEGs were screened according to the criteria of $|\log_2 FC| > 1$, $p < 0.05$ and FDR ≤ 0.05, and subsequent GO analysis and KEGG analyses were performed.

Table 3. Primer sequences used for real-time qualitative PCR.

Gene	Sequence (5′–3′)		Accession number
	Forward primer	Reverse primer	
CYP11A1	TCGCCTTTGAGTCCATCACC	TCCGTCTCAGGTCCCAGTAG	NM_214427.1
CYP19A1	GGGTCACAACAAGACAGGACT	ACCTGGTATTGAAGATGTGTTTTT	NM_214429.1
3βHSD	ACAATCTTACAGGGCCACCC	TGGCCTTTGACCCAGGTTAG	XM_021088745.1
FSHR	CGCGGTTGAACTGAGGTTTG	GCAGGTTGTTGGCCTTTTCA	XM_021085884.1
GAPDH	GGCCGCACCACTGGCATTGTCAT	AGGTCCAGACGCAGGATGGCG	XM_003126531.5

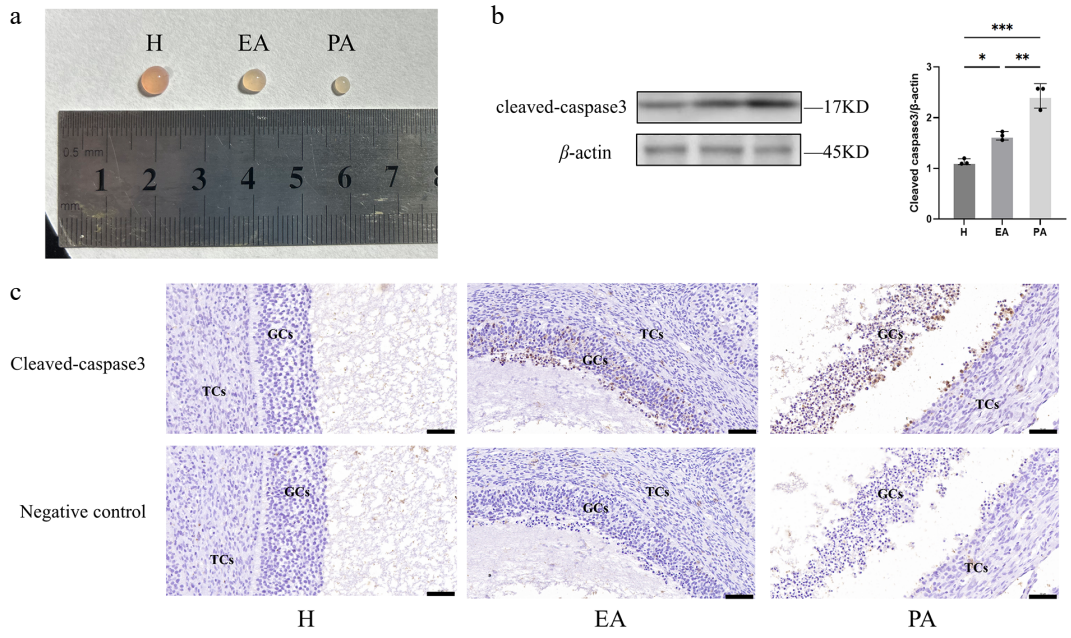

Fig. 1 Follicular morphometric classification and dynamics of GC apoptosis in porcine ovarian follicles. (a) Morphological characteristics distinguishing different types of follicles. (b) Western blot quantification of Cleaved Caspase-3 expression in GC populations. (c) Immunohistochemical staining of Cleaved Caspase-3 in paraffin-embedded follicular sections. H, healthy follicles; EA, early atretic follicles; PA, progressively atretic follicles. Data are represented as the mean ± SEM. Scale bar, 50 μm. *$p < 0.05$, **$p < 0.01$, ***$p < 0.001$.

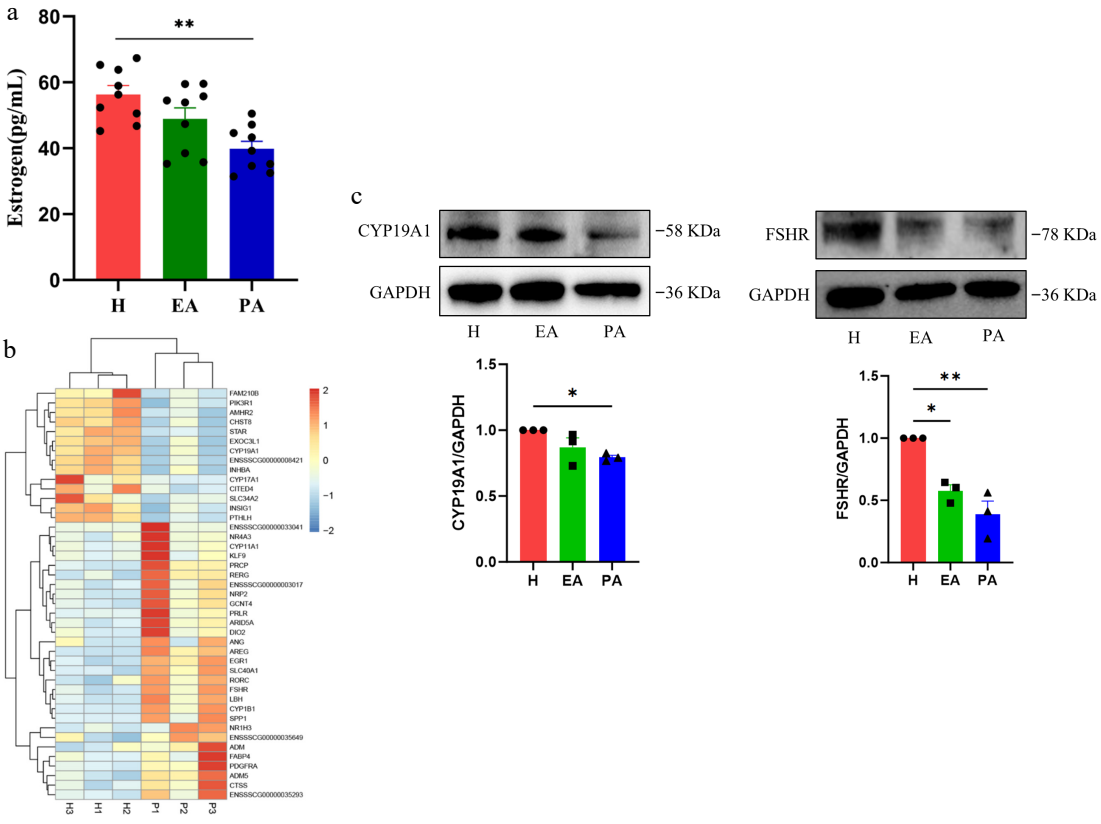

Fig. 2 Estrogen secretion levels in different types of follicles and the expression of hormone secretion-related genes and proteins in granulosa cells. (a) ELISA for estrogen in the follicular fluid of H, EA, and PA. (b) Heatmap of hormone secretion-related genes in granulosa cells of H and PA. Blue, downregulated genes; red, upregulated genes. (c) Western blotting analysis of hormone secretion-related proteins in granulosa cells from H, EA, and PA. H, healthy follicles; EA, early atretic follicles; PA, progressively atretic follicles. Data are represented as the mean ± SEM. * $p < 0.05$, ** $p < 0.01$.

The volcano plot showed that a total of 110 genes were significantly downregulated (blue) and 106 genes were significantly upregulated (red) in the 400 μM SIN-1-treated group (Fig. 5a). Compared with the control group, 762 genes were significantly downregulated (blue) and 979 genes were significantly upregulated (red) in the 800 μM SIN-1-treated group (Fig. 5b).

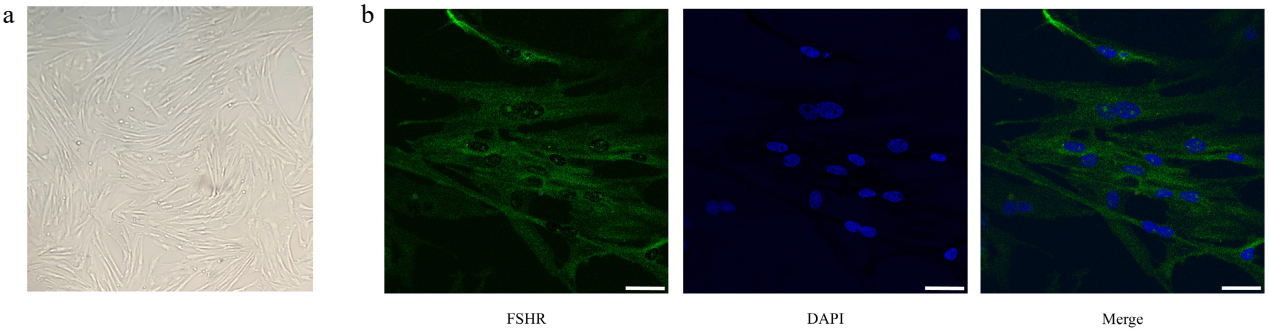

Fig. 3 Morphological observation and purity identification of porcine follicular granulosa cells. (a) Observation of granulosa cells' morphology by inverted microscopy. (b) Immunofluorescence staining of FSHR. From left to right: FSHR fluorescence staining (green); nuclear DAPI staining (blue); merged image. Scale bar, 20 μm.

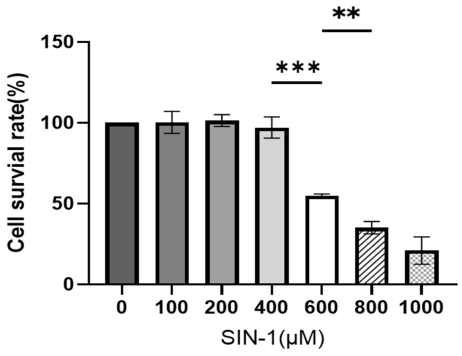

Fig. 4 Cell survival rate of SIN-1-treated granulosa cells. Viability assessment via a CCK-8 assay following 24 h of exposure to SIN-1. Data are presented as the mean ± SEM. ** $p < 0.01$, *** $p < 0.001$.

Functional annotation analysis prioritized the 30 most statistically enriched GO terms and KEGG pathways, with complete inclusion of all terms when the totals fell below 30. Comparative GO analysis of the DEGs between the control and SIN-1-treated groups revealed concentration-dependent functional divergence. Molecular functions, biological processes, and cellular components were the three most gene-enriched terms. The 400 μM SIN-1 group exhibited predominant enrichment in extracellular regions, positive regulation of cell proliferation, and estrogen metabolic processes (Fig. 5c). In contrast, the 800 μM treatment group showed RNA polymerase II regulatory region sequence-specific DNA binding and sequence-specific DNA binding RNA polymerase II transcription factor activity as the dominant functional categories (Fig. 5d). Figure 5e, f displays the *p*-values of the abovementioned GO-enriched terms.

The analysis of the significantly enriched pathways could then be used to understand the main metabolic pathways and signaling pathways associated with the DEGs. In the 400 μM SIN-1 treatment group, DEGs were predominantly enriched in the extracellular matrix (ECM)–receptor interaction, steroid hormone biosynthesis, ferroptosis, and ovarian steroidogenesis pathways (Fig. 5g). In addition, as shown in Fig. 5h, the 800 μM SIN-1 group exhibited predominant enrichment in the cell cycle, the P53 signaling pathway, and the calcium signaling pathway.

OONO⁻ affected estrogen secretion in GCs

To investigate the effects of OONO⁻ on GCs' steroidogenesis, GCs were treated with 400 μM SIN-1 in thesubsequent experiments. ELISA quantification of the supernatants demonstrated a reduction in E_2 secretion in SIN-1-treated GCs compared with the untreated controls (Fig. 6). This suppression occurred despite maintaining cell viability, confirming direct inhibition of steroidogenic capacity rather than secondary cytotoxic effects.

OONO⁻ inhibited steroidogenic gene and protein expression in GCs

To further investigate the effect of OONO⁻ on E_2 secretion in GCs, the RNA-seq data were utilized to screen GO functions containing the terms 'estrogen', 'steroid', and 'hormone'. Significantly different ($p < 0.05$) genes were screened and a heatmap was made (Fig. 7a). Key steroidogenic genes including *CYP11A1* and *3β-HSD* were significantly suppressed. Targeted qPCR validation confirmed reductions in the expression of *CYP19A1* and *3β-HSD* following SIN-1 treatment (Fig. 7b). Western blot analysis demonstrated that the expression of CYP19A1, an E_2 synthesis-related protein, was significantly decreased in the SIN-1-treated group, as well as FSHR (Fig. 7c, d). These results suggest that OONO⁻ affected E_2 synthesis-related genes and proteins in GCs, leading to a decrease in the E_2 secretion capacity of GCs.

The NO scavenger alleviated the effects of OONO⁻ on steroid hormone synthesis

To confirm the specificity of ONOO⁻ in disrupting GC steroidogenesis, cells were co-treated with SIN-1 (400 μM) and the NO scavenger cPTIO (100 μM). ELISA analysis demonstrated partial rescue of E_2 secretion in the cPTIO+SIN-1 groups compared with SIN-1 alone (Fig. 8a). Western blot quantification demonstrated that cPTIO significantly alleviated SIN-1-induced suppression of CYP19A1 and FSHR expression (Fig. 8, c). Given the nitrating activity of OONO⁻, the tyrosine nitration levels in GCs were further evaluated. The results showed that the tyrosine nitration level of GCs was significantly increased after SIN-1 treatment, but the addition of cPITO inhibited this change (Fig. 8d). This further verified that the OONO⁻ produced by SIN-1 inhibits the E_2 secretion capacity of GCs.

Discussion

Synthesis of E_2 by ovarian GCs serves as a critical determinant of follicular competence and female reproductive performance. While prior work established ONOO⁻ as a mediator of GC apoptosis, this study elucidates its novel role in disrupting steroidogenic function.

During follicular atresia, reduced E_2 secretion by GCs was observed. It has also been previously shown that estrogen is essential for proper follicle development[39,40], and low estrogen levels may indicate follicular atresia[41]. This study demonstrated that follicular atresia was associated with significant reductions in both the protein and gene expression levels of E_2 synthesis-related markers (CYP19A1, STAR, and 3β-HSD) in GCs. These changes are temporally correlated with the previously reported elevation of OONO⁻ levels in GCs during follicular atresia[36], suggesting the potential regulatory role of OONO⁻ in suppressing GC-mediated E_2 secretion. To validate this hypothesis, exogenous OONO⁻ administration was experimentally demonstrated to exert multifaceted inhibitory effects on E_2 biosynthesis in GCs.

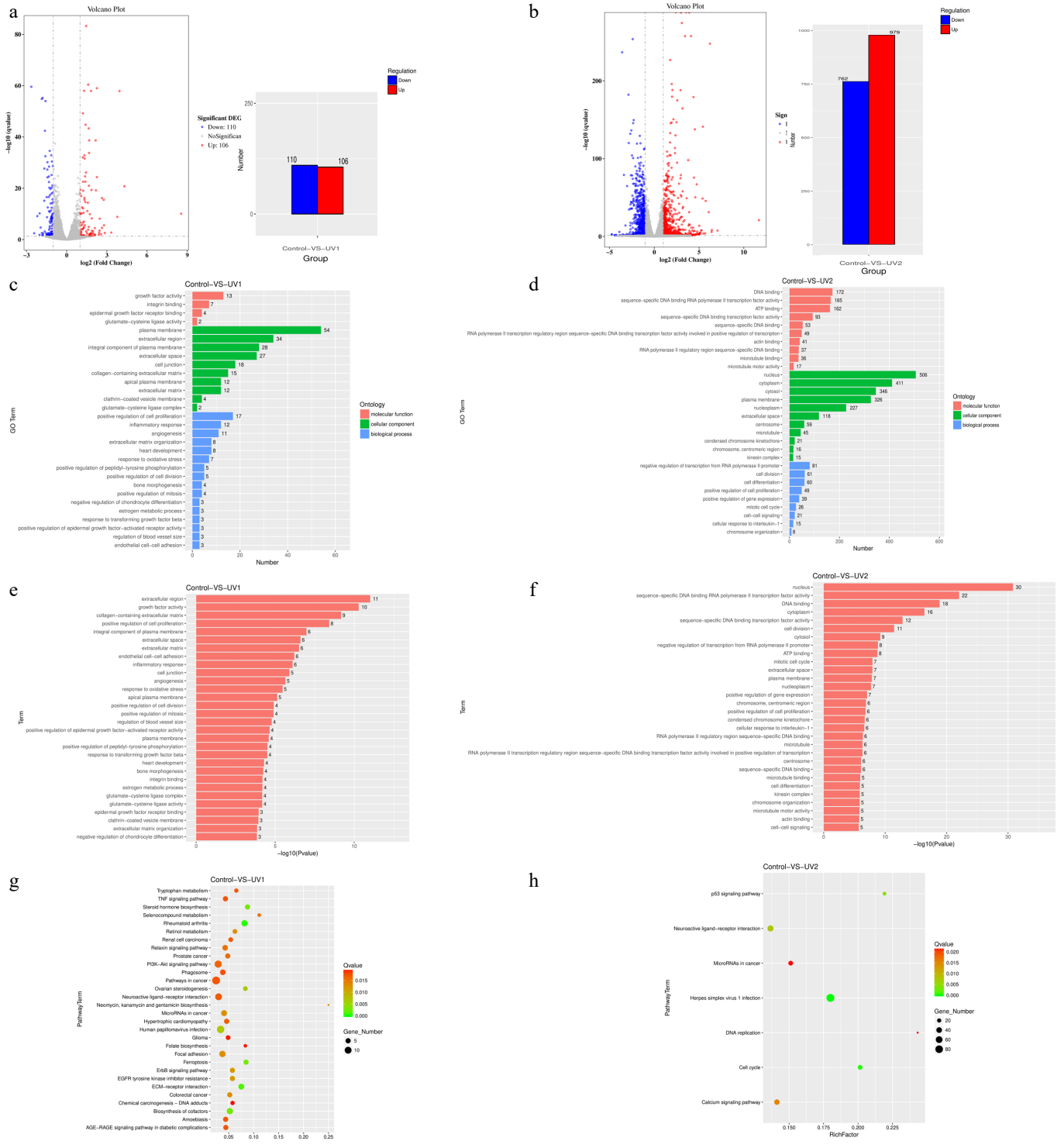

Fig. 5 Number of differentially expressed genes, and GO enrichment and KEGG enrichment of differentially expressed genes in each group after SIN-1 treatment. (a) Volcano plot and bar graph of the DEGs of the 400 μM SIN-1-treated and control groups. The bar graph shows that of all 216 DEGs, 110 of them were downregulated and 106 were upregulated. (b) Volcano plot and bar graph of the DEGs of the 800 μM SIN-1-treated and control groups. The bar graph shows that of all 1741 DEGs, 762 of them were downregulated and 979 were upregulated. For the visualization of the DEGs in the volcano plots. The horizontal coordinate is the fold change in expression in the control and SIN-1-treated groups, and the vertical coordinate is the statistical significance of the change in expression. Different colors indicate different classifications: blue (downregulation), red (upregulation), and gray (no significant difference). (c, d) GO enrichment analysis of DEGs in the control, 400 μM SIN-1-treated, and 800 μM SIN-1-treated groups. The vertical coordinate is the enriched GO term, and the horizontal coordinate is the number of DEGs in that term. Different colors are used to distinguish different enriched terms: blue (biological processes), green (cellular components), and red (molecular functions). (e, f) Statistical significance profiles of GO terms. The vertical coordinate is the enriched GO term and the horizontal coordinate is the *p*-value. (g, h) KEGG enrichment analysis of DEGs in the control, 400 μM SIN-1-treated, and 800 μM SIN-1-treated groups. The vertical coordinate indicates the name of the pathway, the horizontal coordinate indicates the enrichment factor, the dot size correlates with the quantity of DEGs, the color gradient indicates the *q*-value significance. Control, 0 μM SIN-1-treated group; UV1, 400 μM SIN-1-treated group; UV2, 800 μM SIN-1-treated group.

Notably, NO acts as a precursor substance of OONO⁻, which may also be a possible mechanism by which NO affects the E_2 secretion of GCs. It has also been previously shown that excessive NO inhibits the expression of the aromatase protein family[42–44].

Steroid hormones are mainly derived from cholesterol. Prior to hormone synthesis, cholesterol is transferred from the outside to the inside of the mitochondrion by *StAR*[45], and then the conversion of cholesterol to pregnenolone is mediated by *CYP11A1*[46,47], which is then acted upon by *3β-HSD* to synthesize P_4[48]. In addition to its own physiological functions, P_4 is also a precursor for the synthesis of E_2. *CYP19A1* is a key gene in the process of synthesizing E_2. Decreased expression of *CYP19A1* greatly limits E_2 synthesis in GCs[49]. This study demonstrated that OONO⁻ significantly downregulates the expression of 3β-HSD and CYP19A1, which are key enzymes in E_2 synthesis, thereby inhibiting E_2 secretion in porcine ovarian GCs.

FSH is a glycoprotein hormone whose primary function in females is to promote follicular development and maturation, and acts synergically with luteinizing hormone (LH) to induce E_2 secretion and ovulation in mature follicles. FSH acts primarily on GCs. FSHR in GCs is essential for follicular development and E_2 secretion[50], and inhibition of FSHR expression directly affects the biological effects of FSH[51]. Previous studies have reported that FSH acts on FSHR in GCs, which, in turn, modulates the expression of CYP19A1-produced aromatase and stimulates the release of E_2[52–54]. Zhou et al. found that exogenous peroxynitrite may cause tyrosine nitration and proteasome-mediated degradation of FSHR in KGN cells[55]. In this study, the data proved that exogenous addition of SIN-1 decreased the expression level of FSHR protein in GCs, which may be the result of OONO⁻ affecting the expression of FSHR. OONO⁻ inhibits FSHR expression, which may affect the production of aromatase by CYP19A1, and thus affect E_2 secretion. Subsequent experiments demonstrated that SIN-1 elevated total nitration levels in GCs, while its potential induction of FSHR nitration awaits further experimental verification.

In recent years, high-throughput sequencing has been used for bioinformatic analysis in a variety of animals. To further investigate the effects of OONO⁻ on GCs, RNA-seq was used to detect transcriptional differences between GCs in the control, 400 and 800 μM SIN-1-treated groups. GO function and KEGG pathway enrichment analyses allowed the identification of functional or metabolic pathways enriched by the DEGs, which led to speculation about the possible effects of OONO⁻ on GCs. The analytical results revealed that the GO enrichment terms for DEGs under both the 400 and 800 μM treatments included positive regulation of cell proliferation, extracellular space, and the plasma membrane. This suggests that exposure to OONO⁻ at both low and high concentrations alters the expression of GC genes related to proliferation, microenvironment modulation,

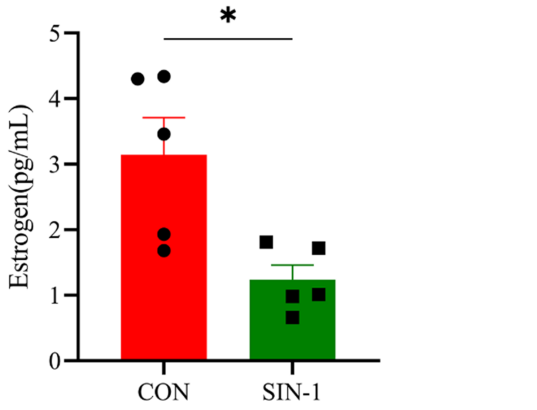

Fig. 6 Hormone secretion levels in SIN-1-treated granulosa cells. Estrogen levels in the cell supernatants tested with an ELISA kit. CON, 0 μM SIN-1-treated group; SIN-1, 400 μM SIN-1 treatment group. Data are presented as the mean ± SEM. * $p < 0.05$, ** $p < 0.01$.

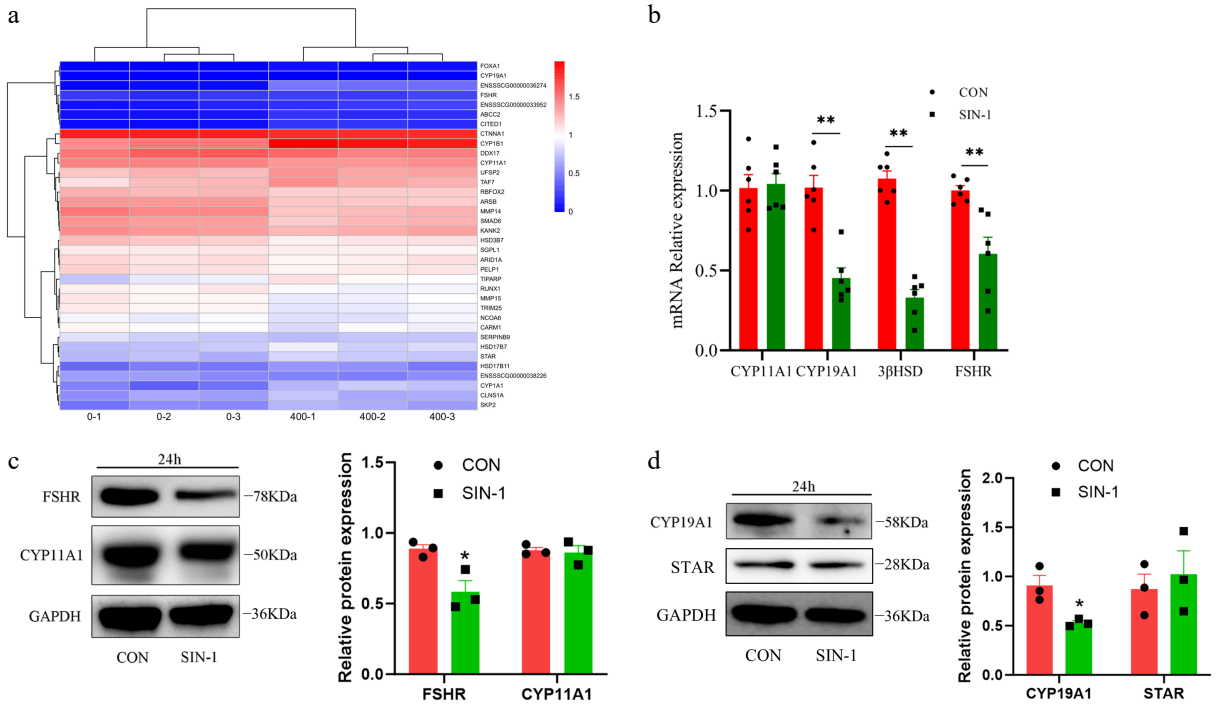

Fig. 7 Expression of hormone secretion-related genes and proteins in granulosa cells. (a) Heatmap of hormone secretion-related DEGs; 0-1, 0-2, and 0-3 are the control groups, whereas 400-1, 400-2, and 400-3 are the 400 μM SIN-1 treatment groups. Blue, downregulated genes; red, upregulated genes. (b) RT-PCR analysis of the relative expression of the mRNA of hormone secretion-related genes in granulosa cells. (c, d) Western blot analysis of hormone secretion-related proteins in granulosa cells. CON, control group; SIN-1, 400 μM SIN-1-treated group. Data are presented as the mean ± SEM. * $p < 0.05$, ** $p < 0.01$.

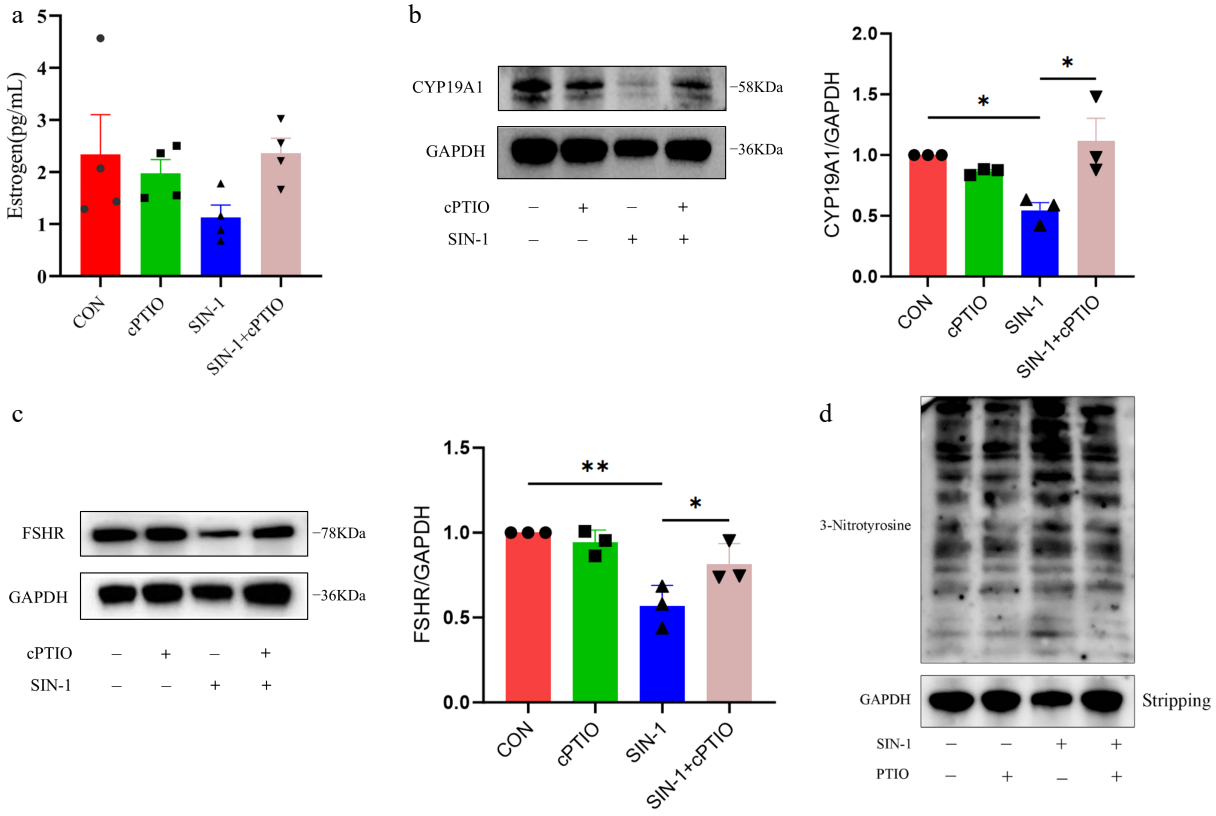

Fig. 8 Levels of E_2 secretion and hormone-related protein expression and overall nitroxylation in granulosa cells. (a) ELISA for estrogen levels in cell supernatants. (b, c) Western blot analysis of hormone secretion-related proteins in granulosa cells. (d) Western blot analysis of total nitroxylation in granulosa cells. Data are presented as the mean ± SEM. * $p < 0.05$, ** $p < 0.01$.

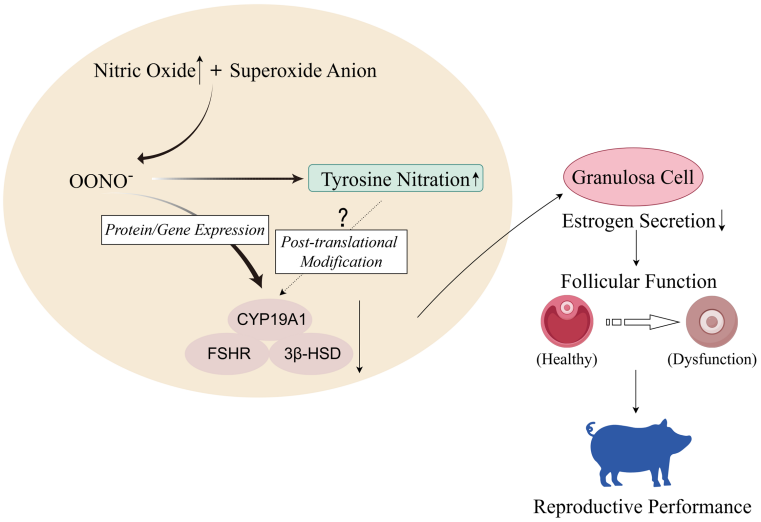

Fig. 9 High concentrations of nitric oxide in organisms react with superoxide anions in reactive oxygen species (ROS) to generate peroxynitrite ions. In porcine ovarian GCs, $OONO^-$ inhibits gene and protein expression of CYP19A1, FSHR, and 3β-HSD, thereby inhibiting GCs' E_2 secretion, leading to ovarian dysfunction and affecting sows' reproductive performance. In addition, $OONO^-$ will also increase the level of tyrosine nitration in GCs, but whether it will cause nitration of hormone synthesis-related proteins needs further experimental verification (figure created with Figdraw).

and intercellular communication, ultimately impairing cellular functionality. In ovarian tissues, the proliferation of GCs is crucial for ovarian function, and impaired GC proliferation may cause follicular dysfunction and, in severe cases, even infertility in females[56]. The extracellular space and plasma membrane function mainly affect intercellular communication as well as the cellular microenvironment. The interactions between oocytes and GCs are very critical during follicular development, as the GCs will create a suitable microenvironment for oocyte development through gap junctions and provide the energy and nutrients required during oocyte development, and oocytes will, in turn, affect the function and differentiation of GCs. It has been found that peroxynitrite inhibits the proliferation and differentiation of human osteoblasts[57]. NO, as a precursor substance of $OONO^-$, is an important signaling molecule in living organisms and plays an important role in intercellular communication. Lillo et al. found that NO causes S-nitrosylation of the cardiac gap junction protein

Connexin-43 (Cx43), which leads to arrhythmias in mice[58]. NO also has the potential to specifically affect Connexin-37 (Cx37), which affects gap junction intercellular communication in human umbilical vein endothelial cells (HUVECs)[59]. Studies have demonstrated that compromised GC functions—including impaired proliferation and dysregulated intercellular signaling—disrupt E_2 secretion. This functional impairment may represent a mechanism through which $OONO^-$ suppresses E_2 biosynthesis.

Notably, DEGs in the 800 μM SIN-1 treatment group exhibited significant enrichment in transcription-related pathways (including RNA polymerase II regulatory region sequence-specific DNA binding and sequence-specific DNA binding RNA polymerase II transcription factor activity, etc.) compared with the 400 μM group. This suggests that excessive $OONO^-$ concentrations may shift cellular regulatory mechanisms from basic metabolic pathways to profound transcriptional-level interventions, potentially through disrupting transcription factor activity to orchestrate the overall regulation of gene expression, which could lead to aberrant epigenetic modifications.

The results of this study demonstrate that DEGs under the high-concentration SIN-1 treatment were primarily enriched in nucleus-, DNA-, and RNA-related functions and pathways compared with the low-concentration treatment, suggesting that higher SIN-1 concentrations may predominantly affect the regulation of genetic material. However, it remains unclear whether this phenomenon arises from cell-autonomous dysregulation of gene expression induced by cytotoxic effects or represents the specific actions of SIN-1 itself. This critical distinction will be systematically investigated in subsequent research.

Conclusions

This study evaluated the effects of $OONO^-$ on GCs' function and E_2 secretion. The RNA-seq results showed concentration-dependent alterations in GCs' functions and pathways. DEGs in GCs treated with 400 μM SIN-1 demonstrated significant enrichment in steroid hormone synthesis. Further studies revealed that the level of E_2 secretion in GCs was decreased at this concentration, and the expression of key steroidogenic proteins and genes was also significantly reduced. In addition, the total nitrification level of GCs was significantly elevated, but the specific effects need to be explored further. In conclusion, these findings indicate that $OONO^-$ may impair GCs' function and inhibit E_2 secretion via modulation of E_2 synthesis-related genes and proteins (Fig. 9).

Ethical statements

All procedures were reviewed and preapproved by the Institutional Animal Care and Use Committee of the Nanjing Agricultural University, identification number: NJAULLSC2020052, approval date: 2020/6/15.

Author contributions

The authors confirm their contributions to the paper as follows: writing – original draft: Zhang Y, Wei Q; investigation: Zhang Y, Lei K; formal analysis: Zhang Y, Lei K, Wang Z; data curation: Zhang Y, Lei K; methodology: Zhao F, Xing J, Zhu S, Li Y, Li S, Ding W, Wei Q; writing – review & editing, supervision, project administration, funding acquisition, and conceptualization: Wei Q. All authors reviewed the results and approved the final version of the manuscript.

Data availability

The high-throughput sequencing data from Figure 5 have been submitted to the NCBI Gene Expression Omnibus (GEO). The BioProject number is PRJNA1248181. This dataset can be accessed at https://dataview.ncbi.nlm.nih.gov/object/PRJNA1248181?reviewer=ejhrbrcc078m4vec1ajc6afrni)

Acknowledgments

This study was financially supported by earmarked funds from the National Natural Science Foundation of China (Nos. 31972565, 32002183, and 31572403), Qinglan Project of Jiangsu Province, and the Science and Technology plan project of Jiangsu Vocational College Agriculture and Forestry (2021kj93).

Conflict of interest

The authors declare that they have no conflict of interest.

References

1. Zhang J, Xu Y, Liu H, Pan Z. 2019. MicroRNAs in ovarian follicular atresia and granulosa cell apoptosis. *Reproductive Biology and Endocrinology* 17:9
2. Hummitzsch K, Anderson RA, Wilhelm D, Wu J, Telfer EE, et al. 2015. Stem cells, progenitor cells, and lineage decisions in the ovary. *Endocrine Reviews* 36:65–91
3. Ma L, Tang X, Guo S, Liang M, Zhang B, et al. 2020. miRNA-21-3p targeting of FGF2 suppresses autophagy of bovine ovarian granulosa cells through AKT/mTOR pathway. *Theriogenology* 157:226–37
4. Zhang Z, Chen CZ, Xu MQ, Zhang LQ, Liu JB, et al. 2019. MiR-31 and miR-143 affect steroid hormone synthesis and inhibit cell apoptosis in bovine granulosa cells through FSHR. *Theriogenology* 123:45–53
5. Hughes FM Jr, Gorospe WC. 1991. Biochemical identification of apoptosis (programmed cell death) in granulosa cells: evidence for a potential mechanism underlying follicular atresia. *Endocrinology* 129:2415–22
6. Zhang X, Chen Y, Yang M, Shang J, Xu Y, et al. 2020. MiR-21-5p actions at the *Smad7* gene during pig ovarian granulosa cell apoptosis. *Animal Reproduction Science* 223:106645
7. Edson MA, Nagaraja AK, Matzuk MM. 2009. The mammalian ovary from genesis to revelation. *Endocrine Reviews* 30:624–712
8. Xie M, Zhang C, Zeng W, Mi Y. 2004. Effects of follicle-stimulating hormone and 17β-estradiol on proliferation of chicken embryonic ovarian germ cells in culture. *Comparative Biochemistry and Physiology Part A, Molecular & Integrative Physiology* 139:521–26
9. Larimore EL, Amundson OL, Bridges GA, McNeel AK, Cushman RA, et al. 2016. Changes in ovarian function associated with circulating concentrations of estradiol before a GnRH-induced ovulation in beef cows. *Domestic Animal Endocrinology* 57:71–9
10. Xing L, Esau C, Trudeau VL. 2016. Direct regulation of aromatase B expression by 17β-estradiol and dopamine D1 receptor agonist in adult radial glial cells. *Frontiers in Neuroscience* 9:504
11. Peluso JJ, Pappalardo A, Losel R, Wehling M. 2005. Expression and function of PAIRBP1 within gonadotropin-primed immature rat ovaries: PAIRBP1 regulation of granulosa and luteal cell viability. *Biology of Reproduction* 73:261–70
12. Rueda BR, Hendry IR, Hendry III WJ, Stormshak F, Slayden OD, et al. 2000. Decreased progesterone levels and progesterone receptor antagonists promote apoptotic cell death in bovine luteal cells. *Biology of Reproduction* 62:269–76
13. Svensson EC, Markström E, Andersson M, Billig H. 2000. Progesterone receptor-mediated inhibition of apoptosis in granulosa cells isolated from rats treated with human chorionic gonadotropin. *Biology of Reproduction* 63:1457–64
14. Lonergan P, Sánchez JM. 2020. Symposium review: progesterone effects on early embryo development in cattle. *Journal of Dairy Science* 103:8698–707
15. Graham JD, Clarke CL. 1997. Physiological action of progesterone in target tissues. *Endocrine Reviews* 18:502–19
16. Knowles RG, Moncada S. 1994. Nitric oxide synthases in mammals. *Biochemical Journal* 298(Pt 2):249–58
17. Ducsay CA, Myers DA. 2011. eNOS activation and NO function: differential control of steroidogenesis by nitric oxide and its adaptation with hypoxia. *Journal of Endocrinology* 210:259–69
18. Guzik TJ, Korbut R, Adamek-Guzik T. 2003. Nitric oxide and superoxide in inflammation and immune regulation. *Journal of Physiology and Pharmacology* 54:469–87

19. Zhang W, Wei QW, Wang ZC, Ding W, Wang W, et al. 2011. Cell-specific expression and immunolocalization of nitric oxide synthase isoforms and the related nitric oxide/cyclic GMP signaling pathway in the ovaries of neonatal and immature rats. *Journal of Zhejiang University SCIENCE B* 12:55–64
20. Ding W, Zhang W, Hui FM, Zhang YH, Zhang FF, et al. 2012. Cell-specific expression and immunolocalization of nitric oxide synthase isoforms and soluble guanylyl cyclase α1 and β1 subunits in the ovary of fetal, neonatal and immature pigs. *Animal Reproduction Science* 131:172–80
21. Basini G, Tamanini C. 2001. Interrelationship between nitric oxide and prostaglandins in bovine granulosa cells. *Prostaglandins & Other Lipid Mediators* 66:179–202
22. Singh VK, Lal B. 2017. Nitric oxide (NO) stimulates steroidogenesis and folliculogenesis in fish. *Reproduction* 153:133–46
23. Tobai H, Nishiya I. 2001. Nitric oxide mediates inhibitory effect of interleukin-1β on estrogen production in human granulosa-luteal cells. *Journal of Obstetrics and Gynaecology Research* 27:53–9
24. Basini G, Grasselli F. 2015. Nitric oxide in follicle development and oocyte competence. *Reproduction* 150:R1–R9
25. Dubey PK, Tripathi V, Singh RP, Saikumar G, Nath A, et al. 2012. Expression of nitric oxide synthase isoforms in different stages of buffalo (*Bubalus bubalis*) ovarian follicles: effect of nitric oxide on *in vitro* development of preantral follicle. *Theriogenology* 77:280–91
26. Chen Q, Yano T, Matsumi H, Osuga Y, Yano N, et al. 2005. Cross-Talk between Fas/Fas ligand system and nitric oxide in the pathway subserving granulosa cell apoptosis: a possible regulatory mechanism for ovarian follicle atresia. *Endocrinology* 146:808–15
27. Zamberlam G, Portela V, de Oliveira JFC, Gonçalves PBD, Price CA. 2011. Regulation of inducible nitric oxide synthase expression in bovine ovarian granulosa cells. *Molecular and Cellular Endocrinology* 335:189–94
28. Virág L, Szabó É, Gergely P, Szabó C. 2003. Peroxynitrite-induced cytotoxicity: mechanism and opportunities for intervention. *Toxicology Letters* 140:113–24
29. Radi R. 2013. Peroxynitrite, a stealthy biological oxidant. *Journal of Biological Chemistry* 288:26464–72
30. Radi R, Peluffo G, Alvarez MN, Naviliat M, Cayota A. 2001. Unraveling peroxynitrite formation in biological systems. *Free Radical Biology and Medicine* 30:463–88
31. Uribe P, Boguen R, Treulen F, Sánchez R, Villegas JV. 2015. Peroxynitrite-mediated nitrosative stress decreases motility and mitochondrial membrane potential in human spermatozoa. *Molecular Human Reproduction* 21:237–43
32. Ottolini M, Hong K, Cope EL, Daneva Z, DeLalio LJ, et al. 2020. Local peroxynitrite impairs endothelial transient receptor potential vanilloid 4 channels and elevates blood pressure in obesity. *Circulation* 141:1318–33
33. Appasamy M, Jauniaux E, Serhal P, Al-Qahtani A, Groome NP, et al. 2008. Evaluation of the relationship between follicular fluid oxidative stress, ovarian hormones, and response to gonadotropin stimulation. *Fertility and Sterility* 89:912–21
34. Franco MC, Ricart KC, Gonzalez AS, Dennys CN, Nelson PA, et al. 2015. Nitration of Hsp90 on tyrosine 33 regulates mitochondrial metabolism. *Journal of Biological Chemistry* 290:19055–66
35. Franco MC, Ye Y, Refakis CA, Feldman JL, Stokes AL, et al. 2013. Nitration of Hsp90 induces cell death. *Proceedings of the National Academy of Sciences of the United States of America* 110:E1102–E1111
36. Lei K, Wei Q, Cheng Y, Wang Z, Wu H, et al. 2023. OONO⁻/MMP2/MMP9 pathway-mediated apoptosis of porcine granulosa cells is associated with DNA damage. *Reproduction* 165:431–43
37. Wei Q, Shi F. 2013. Cleavage of poly (ADP-ribose) polymerase-1 is involved in the process of porcine ovarian follicular atresia. *Animal Reproduction Science* 138:282–91
38. Yousefi S, Soleimanirad J, Hamdi K, Farzadi L, Ghasemzadeh A, et al. 2018. Distinct effect of fetal bovine serum versus follicular fluid on multipotentiality of human granulosa cells in *in vitro* condition. *Biologicals* 52:44–48
39. Dupont S, Krust A, Gansmuller A, Dierich A, Chambon P, et al. 2000. Effect of single and compound knockouts of estrogen receptors α (ERα) and β (ERβ) on mouse reproductive phenotypes. *Development* 127:4277–91
40. Britt KL, Drummond AE, Cox VA, Dyson M, Wreford NG, et al. 2000. An age-related ovarian phenotype in mice with targeted disruption of the Cyp 19 (aromatase) gene. *Endocrinology* 141:2614–23
41. Mukhopadhyay AK, Holstein K, Szkudlinski M, Brunswig-Spickenheier B, Leidenberger FA. 1991. The relationship between prorenin levels in follicular fluid and follicular atresia in bovine ovaries. *Endocrinology* 129:2367–75
42. Banerjee A, Anjum S, Verma R, Krishna A. 2012. Alteration in expression of estrogen receptor isoforms alpha and beta, and aromatase in the testis and its relation with changes in nitric oxide during aging in mice. *Steroids* 77:609–20
43. Vallcaneras S, Morales L, Delsouc MB, Ramirez D, Filippa V, et al. 2022. Interplay between nitric oxide and gonadotrophin-releasing hormone in the neuromodulation of the corpus luteum during late pregnancy in the rat. *Reproductive Biology and Endocrinology* 20:19
44. Masuda M, Kubota T, Aso T. 2001. Effects of nitric oxide on steroidogenesis in porcine granulosa cells during different stages of follicular development. *European Journal of Endocrinology* 144:303–8
45. Jefcoate CR, Lee J. 2018. Cholesterol signaling in single cells: lessons from STAR and sm-FISH. *Journal of Molecular Endocrinology* 60:R213–R235
46. Elustondo P, Martin LA, Karten B. 2017. Mitochondrial cholesterol import. *Biochimica et Biophysica Acta (BBA) – Molecular and Cell Biology of Lipids* 1862:90–101
47. Hu MC, Hsu HJ, Guo IC, Chung BC. 2004. Function of *Cyp11a1* in animal models. *Molecular and Cellular Endocrinology* 215:95–100
48. Coirini H, Gouézou M, Delespierre B, Schumacher M, Guennoun R. 2003. 3 Beta-hydroxysteroid dehydrogenase isomerase (3β-HSD) activity in the rat sciatic nerve: kinetic analysis and regulation by steroids. *Journal of Steroid Biochemistry and Molecular Biology* 85:89–94
49. Oktem O, Akin N, Bildik G, Yakin K, Alper E, et al. 2017. FSH Stimulation promotes progesterone synthesis and output from human granulosa cells without luteinization. *Human Reproduction* 32:643–52
50. Zachos NC, Billiar RB, Albrecht ED, Pepe GJ. 2003. Developmental regulation of follicle-stimulating hormone receptor messenger RNA expression in the baboon fetal ovary. *Biology of Reproduction* 68:1911–17
51. Bhartiya D, Patel H. 2021. An overview of FSH-FSHR biology and explaining the existing conundrums. *Journal of Ovarian Research* 14:144
52. Lai WA, Yeh YT, Fang WL, Wu LS, Harada N, et al. 2014. Calcineurin and CRTC2 mediate FSH and TGFβ1 upregulation of *Cyp19a1* and *Nr5a* in ovary granulosa cells. *Journal of Molecular Endocrinology* 53:259–70
53. Fa S, Pogrmic-Majkic K, Samardzija D, Glisic B, Kaisarevic S, et al. 2013. Involvement of ERK1/2 signaling pathway in atrazine action on FSH-stimulated LHR and CYP19A1 expression in rat granulosa cells. *Toxicology and Applied Pharmacology* 270:1–8
54. de Souza DK, Salles LP, Camargo R, Gulart LVM, Costa ESS, et al. 2018. Effects of PI3K and FSH on steroidogenesis, viability and embryo development of the cumulus-oocyte complex after *in vitro* culture. *Zygote* 26:50–61
55. Zhou G, Hu RK, Xia GC, Yan SH, Ren QL, et al. 2019. Tyrosine nitrations impaired intracellular trafficking of FSHR to the cell surface and FSH-induced Akt-FoxO3a signaling in human granulosa cells. *Aging* 11:3094–116
56. Yamamoto H, Yamashita Y, Saito N, Hayashi A, Hayashi M, et al. 2017. Lower FOXO3 mRNA expression in granulosa cells is involved in unexplained infertility. *Journal of Obstetrics and Gynaecology Research* 43:1021–28
57. da Rocha FAC, de Brum-Fernandes AJ. 2002. Evidence that peroxynitrite affects human osteoblast proliferation and differentiation. *Journal of Bone and Mineral Research* 17:434–42
58. Lillo MA, Himelman E, Shirokova N, Xie LH, Fraidenraich D, et al. 2019. S-nitrosylation of connexin43 hemichannels elicits cardiac stress-induced arrhythmias in Duchenne muscular dystrophy mice. *JCI Insight* 4:e130091
59. Kameritsch P, Khandoga N, Nagel W, Hundhausen C, Lidington D, et al. 2005. Nitric oxide specifically reduces the permeability of Cx37-containing gap junctions to small molecules. *Journal of Cellular Physiology* 203:233–42